Journal of the Meteorological Society of Japan, Vol. 90, No. 2, pp. 207–222, 2012
DOI:10.2151/jmsj.2012-204

Enhanced Mid-Latitude Tropospheric Column Ozone over East Asia: Coupled Effects of Stratospheric Ozone Intrusion and Anthropogenic Sources

Aya NAKATANI, Sayako KONDO, Sachiko HAYASHIDA

Faculty of Science, Nara Women's University, Nara, Japan

Tatsuya NAGASHIMA

Asian Environment Research Group, National Institute for Environmental Studies, Tsukuba, Japan

Kengo SUDO

Graduate School of Environmental Studies, Nagoya University, Nagoya, Japan

Xiong LIU, Kelly CHANCE

Harvard-Smithsonian Center for Astrophysics, Cambridge, MA, United States

and

Isamu HIROTA

Professor Emeritus of Kyoto University, Kyoto, Japan

(Manuscript received 17 March 2011, in final form 27 December 2011)

Abstract

We analyze tropospheric column ozone (TCO) data observed by satellite instruments over East Asia for 15 years (from 1995 to 2009), and investigate the relationship between enhanced TCO (E-TCO) and ozone intrusion from the stratosphere near the subtropical jet (STJ). A belt of E-TCO is observed at mid-latitude over East Asia throughout the year; the belt is located at latitudes approximately equal to that of the STJ on seasonal, monthly, and daily timescales. The observed results are compared with a tagged tracer simulation by using a global chemical transport model. The simulation for East Asia indicates that the contribution from tropospheric origin to the enhancement of TCO is comparable to that from stratospheric origin at latitudes close to the STJ, resulting in the high correlation of the E-TCO belt and the STJ. The two origins of ozone cannot be differentiated in the tropospheric column ozone observed by a satellite, especially over East Asia where the anthropogenic source regions of ozone precursors are situated close to the latitudes of the STJ. Some occasional data, however, indicate split origins on a daily timescale, suggesting that the two origins really contribute to the enhancement of TCO. Our results strongly suggests an urgent need to develop a new satellite sensor and/or a new algorithm to distinguish boundary layer ozone from free tropospheric ozone in order to promote our understanding of atmospheric pollution over East Asia.

1. Introduction

About 90% of atmospheric ozone is in the stratosphere, with tropospheric ozone accounting for only about 10% of the whole amount. Despite its relatively small quantity, however, tropospheric ozone is the primary precursor for hydroxyl (OH) radicals, which control the lifetimes of many gas species in the troposphere. Recently, chemical transport modeling studies have demonstrated that a significant amount of ozone is produced by photochemical processes in the troposphere from anthropogenic ozone precursors and is transported globally, and the roles of photochemical formation processes have been elucidated (Lelieveld and Dentener 2000; Sudo and Akimoto 2007). As a result of its enhancement, tropospheric ozone is the third most important anthropogenic greenhouse gas (Intergovernmental Panel on Climate Change (IPCC) report 2007), and because of its impact on climate change, there is an urgent need to clarify the global and regional behavior of tropospheric ozone. In particular, emissions of ozone precursors, including nitrogen oxide ($NO_x = NO + NO_2$) and volatile organic compounds (VOC), have increased with the rapid economic growth in East Asia (e.g., Ohara et al. 2007). Thus, detailed studies on tropospheric ozone behavior for this region, viewed in association with anthropogenic ozone production, need to be carried out.

Before photochemically produced ozone was evident in polluted regions, it was believed that all tropospheric ozone originated in the stratosphere. Ozone transport from the stratosphere is often associated with the subtropical jet (STJ), typically found at around 200 hPa between 25 and 45°N in the Northern Hemisphere and near 30°S in the Southern Hemisphere. The location of the STJ coincides with an abrupt transition from the tropical tropopause to the mid-latitude tropopause, suggesting that isentropic transverse mass circulations would exchange stratospheric and tropospheric air across this tropopause break (Holton et al. 1995). Recent studies have shown that ozone intrusion from the stratosphere near the STJ strongly influences tropospheric ozone distribution (e.g., Hsu et al. 2005).

Hsu et al. (2005) presented a new diagnostic to determine the stratosphere-to-troposphere flux of ozone utilizing the meteorological fields and a chemistry transport model. They derived the global maps of monthly stratosphere-troposphere exchange (STE) flux and found the STE flux to be most intense around the 20°N–40°N latitudinal belt in May 2000. They found the intense STE flux with about 5–6 g m^{-2} $year^{-1}$ over the Tibetan Plateau, which was extended eastward to China. As described above, East Asia is one of the key regions where both stratospheric intrusion of ozone and anthropogenic ozone production are significant.

Recently, several new methods have been developed to derive tropospheric ozone levels from satellite measurements, making various datasets available. Tropospheric ozone residual (TOR) is one of the techniques for deriving the tropospheric column ozone (TCO). Since the late 1980s, TCO data have been derived by subtracting concurrent measurements of stratospheric column ozone (SCO) from total column ozone (Fishman et al. 1986; Fishman and Larsen 1987; Fishman et al. 1990), and these were further improved afterward (Fishman et al. 2003; Chandra et al. 2003). Most recently, several studies derived TCO from Aura Microwave Limb Sounder (MLS) SCO and Ozone Monitoring Experiment (OMI) measurements by using spatial interpolation (Ziemke et al. 2006), trajectory mapping (Schoeberl et al. 2007), potential vorticity (Yang et al. 2007), and data assimilation (Stajner et al. 2008) to improve the spatial coverage of MLS data. Alternatively, Liu et al. (2005, 2006) derived TCO directly from the spectra obtained by the Global Ozone Monitoring Experiment (GOME).

Satellite measurements have the advantage of continuous and global monitoring. However, as the case stands, satellite measurements are limited to derivation of total tropospheric ozone column, which may mislead the interpretation of tropospheric ozone behavior. For example, Fishman et al. (2003) directly compared the tropospheric column ozone that was derived from the TOR method with population density distribution over Asia, suggesting the effects of anthropogenic activity on ozone production. To clarify the interpretation of extratropical TCO, de Laat et al. (2005) examined contribution of different processes on variability of the TCO by using a chemistry-climate model and revealed the fractional contribution of stratosphere-originating ozone is dominant over extratropics, though the value depends on geographical regions and season. They concluded that the variability of TCO was a very complicated interplay between STE and photochemical ozone formation associated with synoptic-scale system. Though they estimated variability of TCO depending on latitude by analyzing zonal mean values as well as values for each

Corresponding author: Sachiko Hayashida, Faculty of Science, Nara Women's University, Kita-uoya Nishi-machi, Nara 630-8506, Japan
E-mail: sachiko@ics.nara-wu.ac.jp

1°E longitudinal grid, they did not pay much attention to East Asia. As described above, East Asia is a one of the most significant areas for its high emissions of ozone precursors, and thus, detailed analysis of tropospheric ozone in this area is now required from the point of view of hemispheric transport of pollutants.

Hayashida et al. (2008) analyzed the TCO data derived from GOME sensor by Liu et al. (2005) to examine the spatiotemporal variation in TCO over East Asia. Their analysis revealed that the enhanced TCO (E-TCO) belt was observed at mid-latitudes year-round. In this study, we extended the analysis of Hayashida et al. (2008) to investigate the correspondence between the E-TCO belt and the STJ using TCO data observed by satellites and ozonesondes for 15 years (from 1995 to 2009) and meteorological data over East Asia on seasonal, monthly, and daily timescales. In addition to TCO data, we analyzed horizontal wind data from the National Centers for Environmental Prediction/National Center for Atmospheric Research (NCEP/NCAR) reanalysis to investigate the correspondence between the E-TCO belt and the STJ. We also compared the observational data with tagged tracer simulation output from a global chemical transport model, the CHemical Atmospheric general circulation model for the Study of atmospheric Environment and Radiative forcing (CHASER) (Sudo and Akimoto 2007; Nagashima et al. 2010), to assess the contribution of ozone of stratospheric and tropospheric origins.

2. Data description

2.1 GOME

The GOME instrument was launched on 21 April 1995 onboard the European Remote Sensing-2 satellite (European Space Agency 1995). GOME, which observes in nadir view with 40-km along-track and 320-km across-track horizontal resolution, achieving global coverage in three days, provides ultraviolet spectra through observation of solar backscatter for the period from 1995 to the present, but most of its global coverage has been lost due to a data rate limitation since 22 June 2003.

We used the TCO dataset retrieved by Liu et al. (2005, 2006) for the period from 1995 through 2003. In the algorithm of Liu et al. (2005), an ozone profile climatology (McPeters et al. 2003) was used as a priori information, providing ozone mixing ratios at 61 levels from 0 to 60 km for each month and each 10° latitude band. The ozone profiles were derived from GOME measurements in the ultraviolet region (289–339 nm) using an optimal estimation technique. TCO was directly derived using daily tropopause pressures from NCEP/NCAR reanalysis data to divide the stratosphere and troposphere. The daily GOME dataset was provided as swath data for every orbit. Global mean biases and standard deviations of GOME relative to ozonesonde observations were mostly within 3 DU and 3 to 8 DU, respectively (Liu et al. 2005). In this study, we used version 2 of the GOME dataset by gridding the data into sections of 1° × 1.25° in latitude and longitude, and archived the data averaged by seasons, months, and three day periods.

Table 1. Biases (B) and standard deviations of the differences (σ) of the monthly means of tropospheric column ozone (TCO) derived from the Ozone Monitoring Experiment/Microwave Limb sounder (OMI/MLS), in DU. Correlation coefficients (R) between OMI/MLS and ozonesonde data are also shown. See Appendix for the definitions of B and σ.

Station	B	σ	R
Sapporo	0.8	8.5	0.59
Tsukuba	−3.7	6.6	0.71
Kagoshima	−5.1	2.1	0.62
Naha	−1.4	4.6	0.76

2.2 OMI/MLS

The OMI/MLS data were retrieved by Ziemke et al. (2006) by combining measurements from both OMI and MLS instruments onboard the Aura spacecraft, which was launched on 15 July 2004. OMI is a nadir-scanning instrument that detects backscattered solar radiance to measure column ozone with near-global coverage and a resolution of 13 km × 24 km at nadir (Levelt et al. 2006). Total ozone from OMI was derived from the Total Ozone Mapping Spectrometer (TOMS) version-8 algorithm. The MLS instrument is a thermal-emission microwave limb sounder that measures vertical profiles of ozone in the mesosphere, stratosphere, and upper troposphere (Waters et al. 2006).

The OMI/MLS-derived TCO was determined using the TOR method, which consists of subtracting SCO observed by MLS from the total column ozone observed by OMI. For all evaluations of TCO and SCO, tropopause pressure was determined from NCEP/NCAR analysis. Using ozonesondes as a reference, Ziemke et al. (2006) reported that the root-mean-square uncertainties of OMI/MLS data at several ozonesonde sites were about 5 DU. Daily

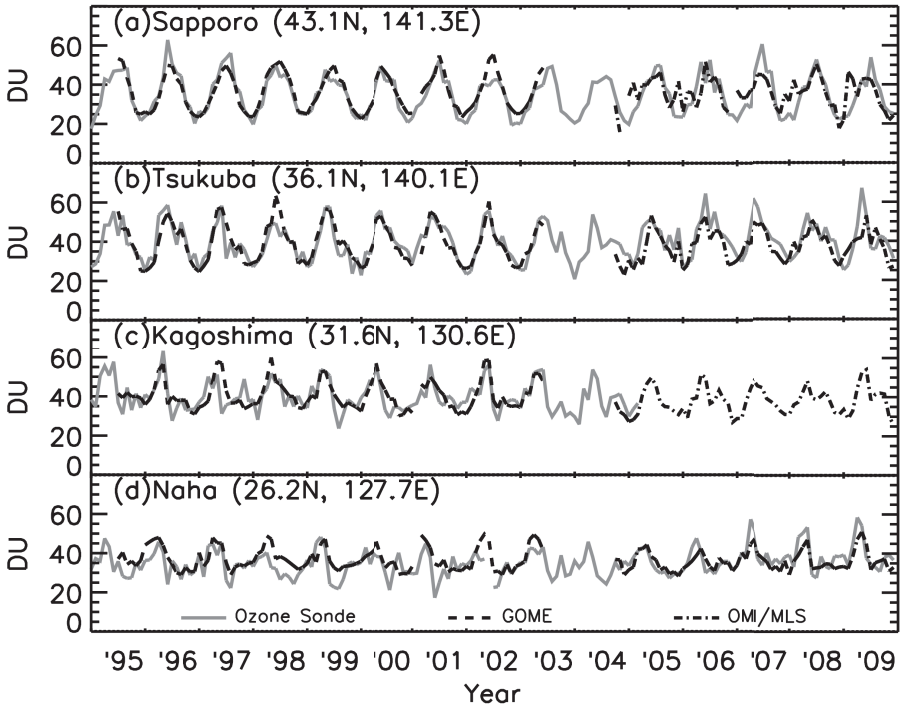

Fig. 1. Time series of monthly means of TCO derived from ozonesondes (shaded curve), GOME (from 1995 through 2003; dashed curve), and OMI/MLS (from 2004 through 2009; dash-dot curve) at (a) Sapporo (43.1°N, 141.3°E), (b) Tsukuba (36.1°N, 140.1°E), (c) Kagoshima (31.6°N, 130.6°E), and (d) Naha (26.2°N, 127.7°E).

and monthly mean OMI/MLS data were gridded to sections of $1^\circ \times 1.25^\circ$ in latitude and longitude within 60°S–60°N and archived on the Internet (http://acdb-ext.gsfc.nasa.gov/Data_services/cloud_slice/new_data.html) for the period from 2004 through 2009. In this study, we analyzed the monthly mean data for the period from 2004 through 2009.

2.3 *Ozonesonde*

The ozonesonde data used in this study were measured by the Japan Meteorological Agency (JMA) at the Sapporo (43.1°N, 141.3°E), Tsukuba (36.1°N, 140.1°E), Kagoshima (31.6°N, 130.6°E), and Naha (26.2°N, 127.7°E) stations; the data are archived at the World Ozone and Ultraviolet Radiation Data Center (WOUDC) web site (http://www.woudc.org). Note that the ozonesonde soundings at Kagoshima ended in March 2005. For consistency with the satellite datasets, we also applied NCEP-based tropopause pressures to derive the TCO from ozonesonde data.

2.4 *Validation of the TCO data derived from satellite measurements*

The GOME- and OMI/MLS-derived TCO data covered different periods. Therefore, to ensure the consistency of both datasets, we validated the GOME and OMI/MLS data using ozonesonde measurements at the four stations in Japan from 1995 to 2009, which were conducted with careful data-quality control by JMA. Noguchi et al. (2007) reported that the GOME (monthly mean) data validation at Japanese stations showed positive biases with a magnitude of only less than 3 DU (∼10%), with the standard deviations relative to ozonesonde observations being only 5–7 DU (∼15–20%). Those results demonstrate that GOME data have sufficient quality by which to study the climatology of tropospheric ozone, such as seasonal variation and regional enhancement.

We applied the same analysis as Noguchi et al. (2007) to the OMI/MLS data. Table 1 shows the biases, standard deviations of the differences, and correlation coefficients of the monthly means of the OMI/MLS data. The period for which there were matching OMI/MLS

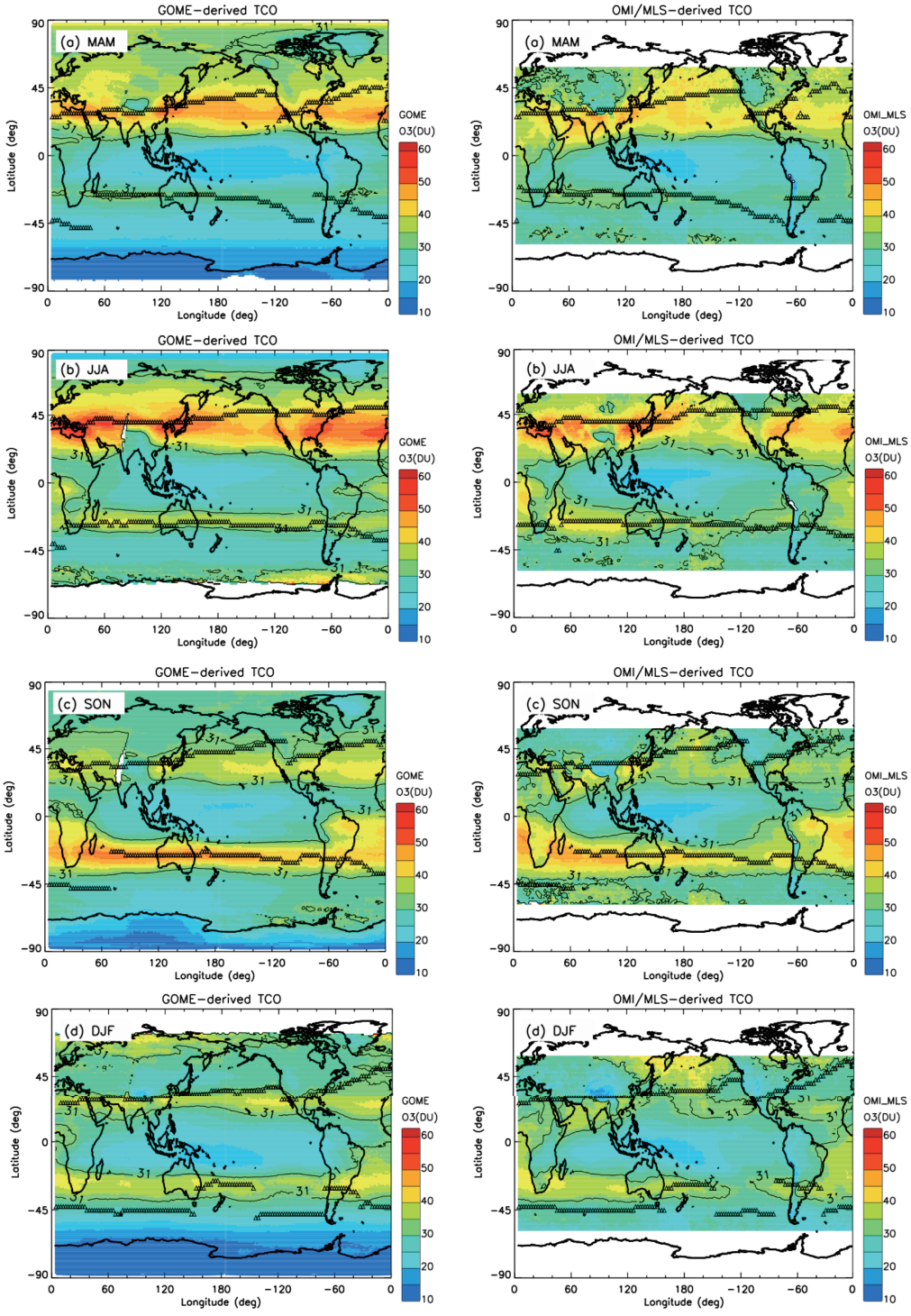

Fig. 2. Seasonal averaged TCO derived from GOME (from 1995 through 2003; left) and OMI/MLS (from 2004 through 2009; right). The triangles represent the location of the subtropical jet (STJ) where the maximum seasonal averaged horizontal wind velocity at 200 hPa occurred. The black contour lines indicate the range of the enhanced TCO (E-TCO) belt where the TCO exceeds 31 DU.

and ozonesonde data at Kagoshima was only six months because the ozonesonde measurements at Kagoshima ended in 2005, resulting in the less reliable bias at Kagoshima than at the other stations.

Compared with the Table 2 of Noguchi et al. (2007), although the standard deviations of OMI/MLS are a little larger than those of GOME, the former are small enough compared with the amplitude of seasonal variation of TCO (approximately 20 DU) and the amplitude of enhancement of TCO that is the focus of this study (approximately 10 DU). In consideration of these comparisons, consistent analysis using both the GOME and the OMI/MLS datasets is possible to discuss the climatological variation in the tropospheric ozone, although discussion of long-term trends is difficult. In this study, we focus on the seasonal variation and regional enhancement of TCO for the past 15 years.

Figure 1 shows the time series of the ozonesonde-, GOME-, and OMI/MLS-derived TCO at each ozonesonde station. Though there were small biases between the GOME or OMI/MLS data and the ozonesonde-derived TCO, as shown in Table 1, two satellite-derived TCOs showed the same phases of seasonal variation in ozonesonde-derived TCO. As previously reported by Hayashida et al. (2008), the different phases in TCO among the four ozonesonde stations (i.e., a station at higher latitude peaked later) were also observed in OMI/MLS data.

3. Results

3.1 Comparison of GOME and OMI/MLS data

In this section, we discuss the global maps of TCO observed by GOME and OMI/MLS; in later sections, we focus on East Asia. Figure 2 shows global maps of the seasonal average TCO derived from GOME (left) and OMI/MLS measurements (right). The GOME data were averaged over ∼9 years from 1995 through 2003, whereas the OMI/MLS data were averaged over ∼5 years from 2004 through 2009; the averaged terms were long enough to obtain reliable climatology. The OMI/MLS maps show similar features to those found in GOME data. In the Northern Hemisphere, particularly high concentrations of TCO were observed over the Mediterranean Sea, the Middle and Near East, East Asia, North America, and the North Atlantic. In the tropics, enhancement of TCO over the tropical Atlantic Ocean between South America and Africa is substantial in contrast to the low TCO over the Pacific. This is a well-known wave-1 pattern, which has been reported over the tropics in previous studies (e.g., Fishman et al. 1990; Thompson and Hudson 1999). We define the E-TCO belt as the area where TCO exceeded 31 DU at mid-latitudes; the threshold value was determined as 31 DU because the mean value of TCO for the area between 60°S and 60°N during the observation period was about 31 DU for both the GOME and OMI/MLS datasets. In Fig. 2, the black contour lines indicate the threshold value of 31 DU.

Figure 2 also shows the latitude of the STJ (L_{STJ}), at which the horizontal wind velocity reached a maximum of 200 hPa. In all seasons, the STJ was situated between about 25° and 45° in both hemispheres. Although the enhancement of TCO corresponds to the STJ in most areas, it is not the case over the tropical Atlantic Ocean between South America and Africa. The discrepancy was most notable in September–October–November (SON). Numerous studies have revealed that TCO was enhanced in this area during SON because of increased ozone precursors emitted by lightning and biomass burning (e.g., Krishnamurti et al. 1996; Pickering et al. 1996; Wang et al. 1998; Lelieveld and Dentener 2000; Andreae et al. 2001; Meyer-Arnek et al. 2005; Martin et al. 2002; Sauvage et al. 2007).

On the other hand, over East Asia, the E-TCO belt is located at approximately the same latitude as the STJ throughout the year. In the following section, we focus on the seasonal variation in the E-TCO belt and the STJ over East Asia in more detail.

3.2 Seasonal variation of the STJ and the E-TCO belt over East Asia

Hereafter, we describe the latitude of the E-TCO belt ($L_{E\text{-}TCO}$) as the latitude of maximum TCO along a longitude. As shown in Fig. 2, the E-TCO distribution has generally a zonal structure and $L_{E\text{-}TCO}$ does not depend significantly on the longitude between 100 and 170°E. In this analysis, 130°E was taken as the representative longitude for the analysis area of East Asia.

Figure 3 shows a time-latitude cross-section of GOME and OMI/MLS data along 130°E, calculated as the running mean along the latitude every 10°. The asterisks indicate $L_{E\text{-}TCO}$. This figure extends the period in Fig. 2a of Hayashida et al. (2008) to after 2004 as covered by OMI/MLS. The E-TCO belts observed by GOME and OMI/MLS showed similar seasonal variation, although the concentration and amplitude of the E-TCO belts differed from year to year. The E-TCO belt moved north from March to August and south from September to February within 25–45°N.

As previously reported by Hayashida et al. (2008), the E-TCO belt was located near the latitudes of Tsukuba (36.1°N) and Kagoshima (31.6°N); the E-TCO belt was rarely situated at Sapporo (43.1°N) and Naha (26.2°N) throughout the year (Fig. 3). The observations

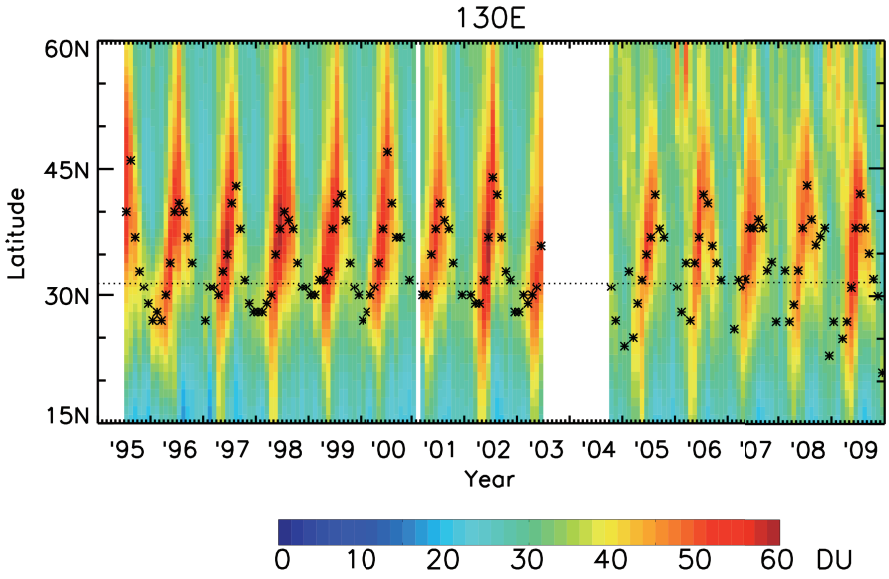

Fig. 3. Time-latitude cross-section of TCO derived from GOME (from 1995 to 2003) and OMI/MLS (from 2004 to 2009) along 130°E. Asterisks indicate the latitude of the maximum TCO (latitude of the E-TCO: $L_{E\text{-}TCO}$). Dashed lines correspond to the latitudes of Kagoshima.

in the lower troposphere at Tsukuba were influenced by air pollution from nearby Tokyo (e.g., Logan 1999). For these reasons, we here show ozonesonde data at Kagoshima, which is close to the latitude of the E-TCO belt and not affected by local air pollution. Figure 4a shows the time series of L_{STJ} (gray) and $L_{E\text{-}TCO}$ (black) on a monthly basis. The $L_{E\text{-}TCO}$ observed by both satellites was close to L_{STJ} throughout the entire period as shown in this figure. If the intrusion of stratospheric ozone enhanced TCO, ozone at high altitudes would increase more than that at lower altitudes when TCO was enhanced. As these satellite data either provide column ozone data or do not have adequate vertical sensitivity, we analyzed the ozonesonde data to determine the vertical distribution.

Figure 4b shows the time series of ozonesonde-derived TCO at Kagoshima divided into layers at 200-hPa intervals. Among the layers shown in Fig. 4b, the ozone in the uppermost two layers (above 400 hPa) is indicated by the thick curve in Fig. 4c, and its contribution ratio to TCO is given by the thin curve. The dashed line in Fig. 4a corresponds to the latitude of Kagoshima (31.6°N). The period when the STJ was located within ±2.5° (one grid of NCEP/NCAR data) of Kagoshima is shaded in gray. The shaded area covers 58 months. As the STJ and the E-TCO belt were located close to each other, the shaded areas also correspond to the periods when the E-TCO belt was located near Kagoshima. During these periods, the ozonesonde-derived TCO at Kagoshima increased as shown in Fig. 4b. During the period indicated by the shaded gray region in Fig. 4, ozone at high altitudes (especially above 400 hPa) increased significantly, as shown in Fig. 4c, suggesting that the upper tropospheric ozone was associated with the enhancement of TCO during the shaded periods and indicating the effects of stratospheric ozone intrusion. However, the contribution ratio of upper tropospheric ozone between 400 hPa and the tropopause is not statistically dominant compared with the contribution of lower tropospheric ozone: the two contributions are almost comparable.

3.3 Comparison of short-term variability between three-day averaged horizontal wind and GOME data

Figures 2 to 4 show that the E-TCO belt and the STJ were located at similar latitudes on seasonal and monthly timescales over East Asia. However, the processes that cause the intrusion of stratospheric ozone into the troposphere proceed on a shorter (daily) timescale (Holton et al. 1995). As the ozonesonde measurements are limited to only about four times a week, TCO shown on a monthly basis as shown in Figs. 4b and 4c may not necessarily reflect the events of

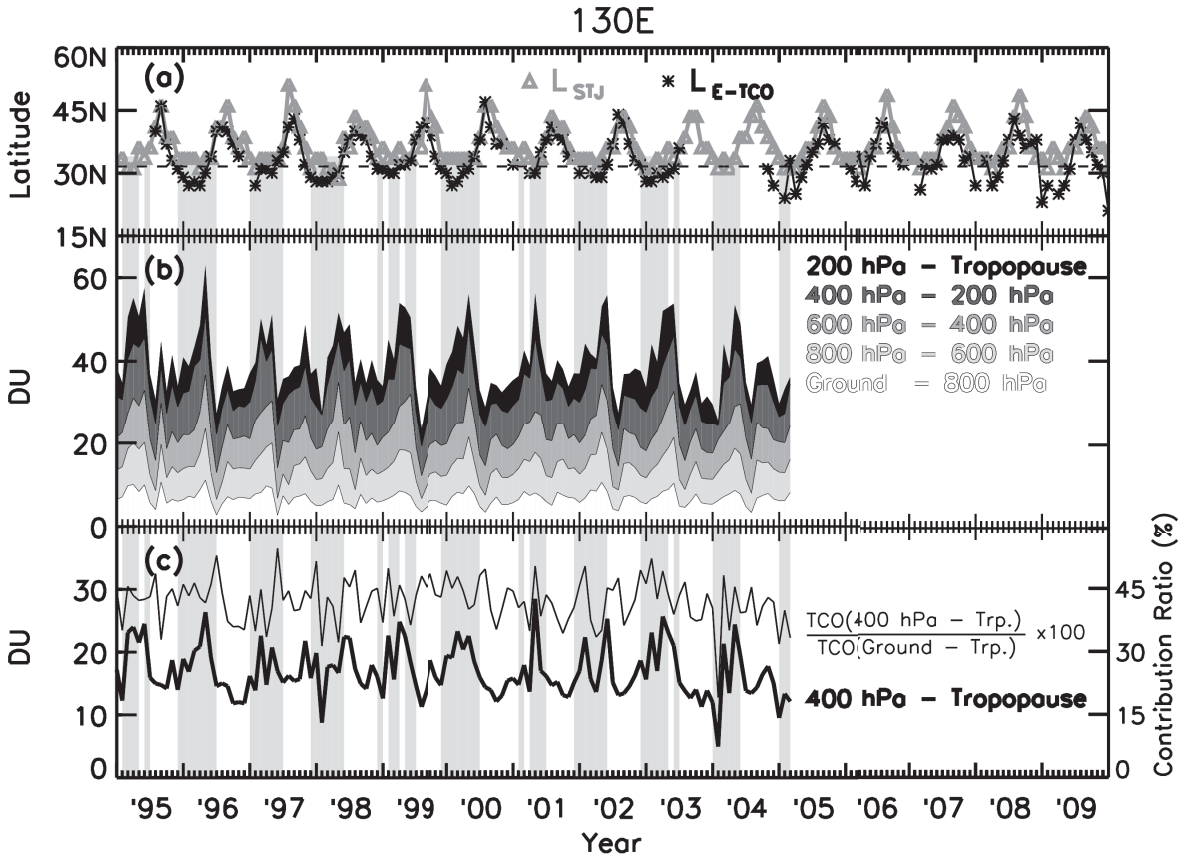

Fig. 4. (a) Time series of L_{STJ} (gray) and $L_{E\text{-}TCO}$ (black) at 130°E. The values of $L_{E\text{-}TCO}$ were obtained by GOME data during the period from 1995 to 2003 and by OMI/MLS data from 2004 to 2009. The dashed line corresponds to the latitude of Kagoshima (31.6°N). (b) Time series of the ozonesonde-derived TCO at Kagoshima divided into layers at 200-hPa intervals: ground–800, 800–600, 600–400, 400–200, and 200 hPa–tropopause. No data were available after March 2005. (c) Time series of the ozonesonde-derived TCO integrated from 400 hPa to tropopause (thick curve, scale on left) and its contribution ratio to TCO (thin curve, scale of right). The period when the STJ was located within ±1 grid of Kagoshima is shaded gray.

ozone intrusion from the stratosphere. For the shorter timescale analysis, we constructed three-day-average maps of TCO and horizontal wind velocity in 2002; the three-day period was the shortest timescale in which the GOME covered the entire globe. All the TCO maps based on 2002 data for the three-day timescale were examined (figures are not shown).

Figure 5a shows a representative example obtained from 16 to 18 July 2002, though all of the data cannot be shown here. For these three days, only a few data points for GOME retrievals were missing; thus, the E-TCO belt was identified clearly as shown in the right panel of Fig. 5a. The STJ was located around 40°N and meandered near the Korean Peninsula (∼40°N, 130°E; left panel of Fig. 5a). The distribution of the E-TCO area had a pattern of meandering similar to that of the STJ. Highly concentrated TCO was observed near the Korean Peninsula where the axis of the STJ meandered. The correspondence between high concentrations of TCO and meandering of the STJ suggests that the ozone intrusion from the stratosphere was associated with the passage of a trough. On other days in 2002, the distribution of E-TCO showed a pattern similar to that of the STJ, although the distribution patterns varied day by day suggesting that the enhancement of TCO was partly attributable to ozone transport from the stratosphere.

There were also days when E-TCO showed a distri-

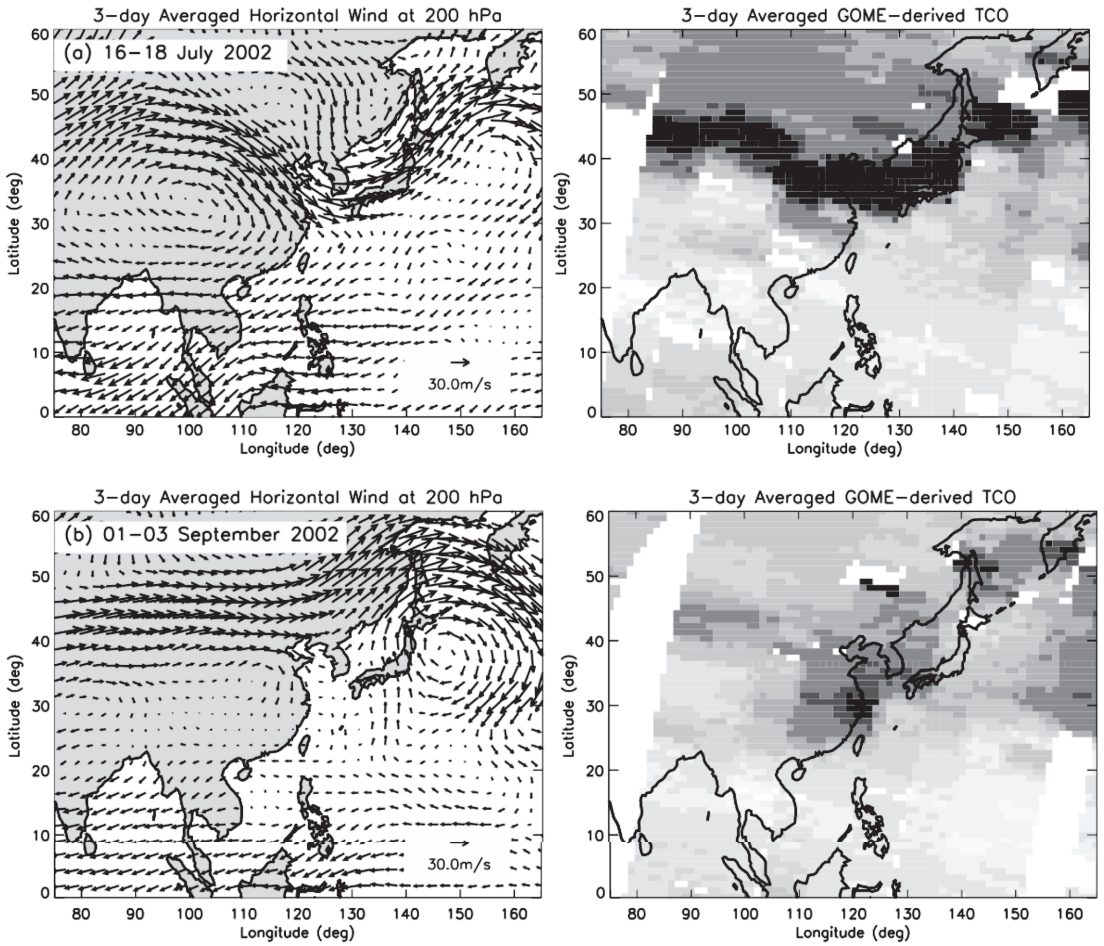

Fig. 5. Three-day averaged horizontal wind at 200 hPa (left) and three-day composite of the TCO map observed by the GOME (right): (a) 16–18 July 2002; (b) 1–3 September 2002.

bution pattern that differed from that of the STJ. Figure 5b is an example of such a case on 1–3 September 2002. This is the only example clearly showing different distributions for E-TCO and the STJ in 2002. The STJ was observed around 45°N (left panel of Fig. 5b). The TCO map of the GOME data also showed a band of E-TCO with about 40 DU at the same latitude (∼45°N) as the STJ. Except for the band of E-TCO around 45°N, TCO enhancement of about 50 DU was also observed over the eastern shore of China (110–130°E, 25–40°N); the distribution of the TCO pattern differed from that of the STJ. This enhancement of TCO over China was observed for about two weeks, after which the E-TCO moved eastward and diminished. This kind of short-lived event for E-TCO was not discernible in monthly mean data.

4. Tropospheric column ozone calculated by the chemical transport model CHASER

4.1 Overview of CHASER

The observational data were compared with a tagged tracer simulation (Sudo and Akimoto 2007; Nagashima et al. 2010) using the global chemical transport model CHASER (Sudo et al. 2002). For this study, the horizontal resolution of T63 (∼1.9 × 1.9 degrees) was adopted with 32 vertical layers from the surface to an altitude of ∼40 km. For the tracer tagging, we separated the model domain into 45 source regions, which included 22 regions in both the planetary boundary layer (PBL) and in the free troposphere (FT) as well as the entire stratosphere. We then calculated the distribution of hypothetical ozone tracers, each of which was allowed to be chemically produced only inside its designated

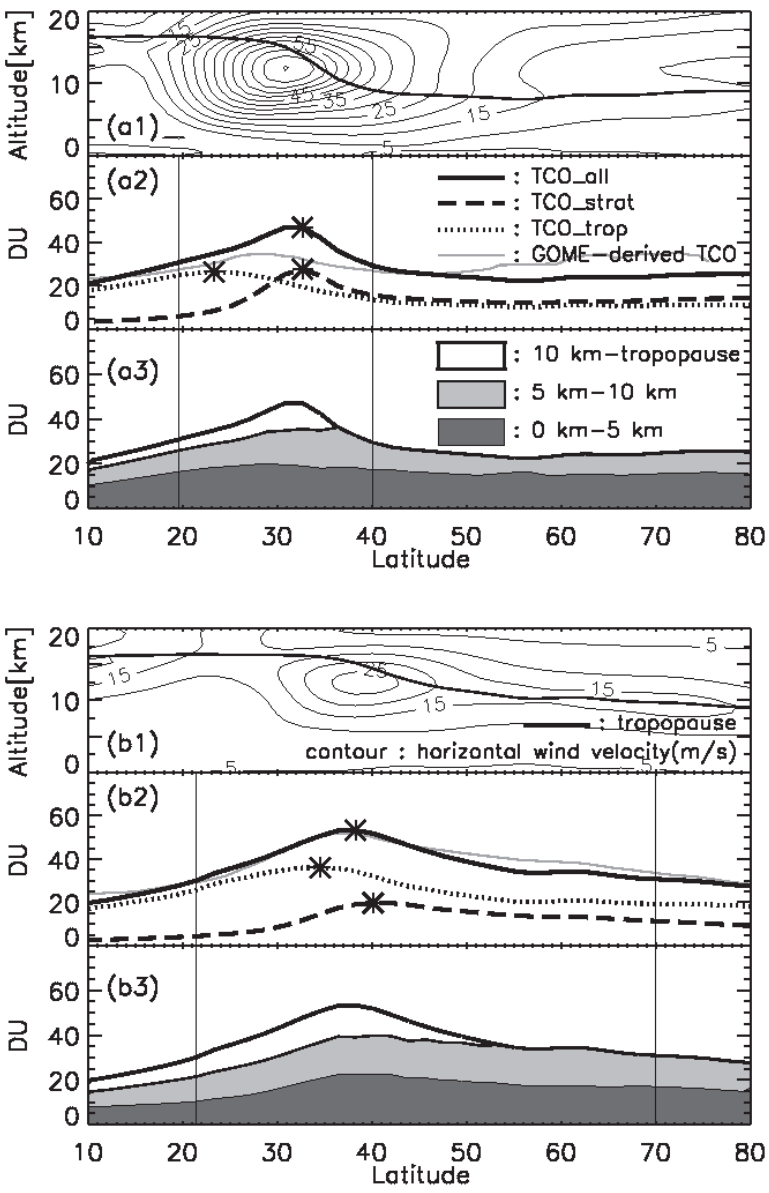

Fig. 6. Upper panels (a1) (a2) (a3) depict the mean values for winter (December, January, and February) from 2000 to 2005. All values are averages from 112°E to 131°E. (a1) Latitude-altitude cross-section of tropopause height (thick curve) and horizontal wind velocity (contour lines). (a2) Latitudinal profile of seasonal mean ozone with contributions from the stratosphere (TCO_strat, dashed curve), troposphere (TCO_tropo, dotted curve), and total tropospheric column ozone (TCO_all, black thick curve) calculated by the model. Asterisks indicate each maximum value. Vertical lines indicate the latitude at which TCO_all was 31 DU (i.e., the area between the two vertical lines is the E-TCO belt). The gray curve shows seasonal mean GOME data. (a3) Latitudinal profile of TCO_all divided into 5-km intervals: TCO at 0–5 (dark gray), 5–10 (light gray), and 10 km–tropopause (white). Lower panels (b1) (b2) (b3) are the same as (a), but for summer (June, July and August) from 2000 to 2005.

source region. Thus, the concentration of each ozone tracer tagged by its source region represented the contribution of that source region. The detailed procedure has been described by Nagashima et al. (2010).

Model simulations were conducted for six years from 2000 to 2005. The model meteorological field (horizontal wind velocities and temperatures) from the NCEP/NCAR reanalysis six-hour data of the corresponding year was assimilated into CHASER. CHASER, which focuses on tropospheric chemistry, does not include halogen chemical systems that are important to stratospheric chemistry, and consequently overestimate the concentration of stratospheric ozone. In order to improve the overestimation of stratospheric ozone, monthly mean concentrations of ozone and some nitrogen compounds (NO_x, HNO_3, and N_2O_5) calculated by other chemistry climate model, which includes a whole set of stratospheric halogen chemistry, were assimilated into CHASER above the tropopause. The stratospheric chemistry climate model data for the assimilation were taken from Akiyoshi et al. (2009) for ozone and Takigawa et al. (1999) for the nitrogen compounds.

4.2 Source attribution of the modeled TCO

We divided the total tropospheric column ozone (TCO_all) into stratospheric and tropospheric origins. The modeled TCO of stratospheric origin is referred to as "TCO_strat," and photochemically produced ozone in the troposphere is referred to as "TCO_tropo" (i.e., TCO_all = TCO_strat + TCO_tropo). Figure 6a shows (a1) the model meteorological field (tropopause and horizontal wind velocity) and (a2) the modeled TCO (TCO_all (black curve), TCO_strat (dashed curve), and TCO_tropo (dotted curve)) which were averaged from 2000 to 2005 and from 112° to 131°E in winter (December–January–February, DJF). Figure 6b shows the same for summer (June–July–August, JJA). The gray curve in Figs. 6a2 and b2 give the seasonal averaged GOME data. The asterisks in Figs. 6a2 and b2 represent maximum values of TCO_all, TCO_strat, and TCO_tropo. The vertical lines (in Figs. 6a2, 6a3, 6b2, 6b3) represent the latitude at which TCO_all was 31 DU. According to the definition used in this study, the areas where TCO_all exceeded 31 DU are determined as the modeled E-TCO belt (between the two vertical lines). As defined for satellite data, the latitude where TCO_all is at a maximum (L_{TCO_all}) is the latitude of the modeled E-TCO belt.

As shown in Figs. 6a2 and b2, TCO_tropo was the dominant source of E-TCO (TCO_tropo $\geq$ TCO_strat). Contribution ratios of TCO_tropo to TCO_all within the area of the modeled E-TCO belt were greater than those of TCO_strat: 56% in winter and 67% in summer.

Note that the peak latitude of TCO_strat (L_{TCO_strat}) shifts from around 33°N in winter to around 40°N in summer along with the northward shift of L_{STJ} from winter to summer, resulting from the extension of the Hadley circulation. The peak latitude of TCO_tropo (L_{TCO_tropo}) also shifts northward from winter to summer. When the detailed origins from the tagged simulation are examined, tropospheric ozone originates from remote regions such as a biomass burning region (e.g., Southeast Asia) in winter, whereas in summer the ozone produced in China increases at around 35°N (figures for different origins are not shown). Thus, both L_{TCO_tropo} and L_{TCO_strat} shift northward from winter to summer, resulting in the shift of L_{TCO_all} from around 33°N in winter to around 38°N in summer. Although the contribution of TCO_tropo to the enhanced ozone is comparable with or even greater than that of TCO_strat, L_{TCO_all} moves along with the latitude of the STJ because TCO_strat has a steeper latitudinal gradient than does TCO_tropo. This may mislead the interpretation to one where the enhancement of TCO could be attributed to only the intrusion of stratospheric ozone.

Figure 6a3 shows the modeled TCO divided into layers at 5-km intervals for winter (DJF), whereas Fig. 6b3 shows the same but for summer (JJA). The contribution from the upper troposphere between 10 km and the tropopause to the total amount of TCO is significant near the L_{STJ} as expected. The simulations shown here are consistent with the observation at Kagoshima (Figs. 4b, c) as described in the previous section.

5. Discussion

Satellite measurements are useful for observing the spatiotemporal variation of tropospheric ozone, as they have the advantage of continuous and global monitoring. However, satellite measurements can provide basically only the column amount of ozone without information regarding the vertical distribution of ozone. Recently, some thermal infrared sensors, such as the Tropospheric Emission Spectrometer (TES), demonstrated that they are able to detect relative variations in the coarse vertical structure of tropospheric ozone (e.g., Worden et al. 2007). In most cases, however, they do not have adequate vertical sensitivity to dissociate the stratospheric effect and the photochemical effect on tropospheric ozone burden. East Asia is a region where both intrusion of stratospheric ozone and anthropogenic ozone production in the lower troposphere affect the tropospheric ozone burden significantly. Thus, the interpretation of satellite TCO data analysis is difficult.

As mentioned in Section 4, the observed features of TCO presented in Section 3 can be interpreted as follows:

- The contribution of troposphere-originating ozone to the enhanced ozone is almost comparable to that of stratosphere-originating ozone.
- The increase in the upper tropospheric ozone near the STJ is attributable to the ozone intrusion from the stratosphere. The peak latitude of stratosphere-originating ozone shifts to around 40°N in summer along with the shift of the STJ polewards in summer.
- Troposphere-originating ozone over East Asia is produced in different remote regions depending on the season. Transport from Southeast Asia (possibly due to biomass burning) is dominant in winter, whereas photochemical production over China is dominant source in summer. The latitudinal distribution of troposphere-originating ozone is rather flat compared with stratosphere-originating ozone.
- As the results show, the peak latitude of the E-TCO belt (L_{TCO_all}) moves in association with STJ latitude. Although L_{TCO_all} moves along with the latitude of the STJ because TCO_strat has a steeper latitudinal gradient than does TCO_tropo, this may mislead the interpretation to one where the enhancement of TCO could be attributed only to the intrusion of stratospheric ozone.

The results shown in Figs. 2 to 4 are all obtained by analysis of seasonal and monthly data. As mentioned in Subsection 3.3, there are some cases showing a short-lived event of ozone enhancement in East Asia. The three-day composite of the GOME-derived TCO (Fig. 5b) over East Asia also showed different distribution patterns for E-TCO and the STJ for approximately a two-week period. This event did not appear in monthly mean data because of its short lifetime. The ozone enhancement can be attributed to photochemical production due to anthropogenic emissions. In particular, emissions of ozone precursors (e.g., NO_x and VOC) have increased in urban areas concentrated along the eastern seaboard of China (e.g., Streets et al. 2003, Zhang et al. 2009). In the Northern Hemisphere, especially in East Asia, the source regions of anthropogenic ozone precursors are close to the location of the STJ. Our results suggest that photochemically produced ozone must be masked by ozone of stratospheric origin in TCO observations from satellites over East Asia. The results of this study will give an important perspective to a future plan of monitoring of atmospheric environment over East Asia from Geostationary Environment Monitoring Spectrometer (GEMS) onboard MP-GEOSAT (Multi Purpose Geostationary Satellite) that is being planned by KARI (Korea Aerospace Research Institute) (e.g., Lee 2009).

As to CHASER tagged-simulation, a quantitative discussion may not be sufficiently reliable at present. Stevenson et al. (2006) summarized the stratosphere-troposphere exchange (STE) of ozone calculated from 26 atmospheric chemistry models, and showed that there is a large variety in estimates for stratospheric ozone input fluxes ranging from 296 to 930 $Tg(O_3)$ $year^{-1}$ (see Table 5 in Stevenson et al. (2006)). In their intercomparison and also in the analysis in Sudo and Akimoto (2007), CHASER was reported to give a value for stratospheric ozone input of about 500 $Tg(O_3)$ $year^{-1}$. In the tagged-tracer simulation with CHASER used in this paper (Nagashima et al. 2010), the stratospheric ozone input is estimated to be about 135 $Tg(O_3)$ $year^{-1}$. This estimation for stratospheric ozone input is lower than the range shown in Stevenson et al. (2006). However, it is difficult to evaluate the reliability of the model estimation of the ozone input because the value depends significantly on the individual model, conditions of calculation, and how it is calculated. In the tagged-tracer simulation used in this study, the concentration of ozone calculated by a stratospheric chemistry climate model was assimilated into CHASER above the tropopause. If we assimilated the ozone concentration only above 55 hPa (∼20 km) altitude as in Sudo and Akimoto (2007), stratospheric ozone input would be estimated to be about 560 $Tg(O_3)$ $year^{-1}$, which well falls within the range shown in Stevenson et al. (2006). However, comparisons between the calculated concentrations of ozone with the several ozonesonde observations revealed that the simulation limiting the assimilation of stratospheric ozone above 55 hPa obviously overestimated the concentration of ozone, particularly at the upper troposphere. On the other hand, the tagged-tracer simulation used in this study showed better ability to simulate the ozonesonde observations in the entire troposphere, including the upper troposphere where the concentration of ozone would be largely influenced by the stratospheric ozone input. That said, this should not legitimate the low ozone input flux used in this study. In fact, the budget analysis of tropospheric ozone is still a scientific topic under investigation. However, even if the stratospheric ozone input flux used in this study was underestimated, the relative variation would be reasonable to interpret the behavior of observed E-TCO quali-

tatively as described above.

Note that the tropopause height should be determined carefully because the gradient of ozone profile near the tropopause is extremely steep. As mentioned in Section 2, we utilized the NCEP tropopause height when integrating the ozone profile up to the tropopause just to keep consistency with analysis of satellite data. To confirm the effect of tropopause height definition, we also estimated TCO by integrating up to the tropopause height determined from ozonesonde temperature measurements. When temperature profiles show double tropopauses, ozone was integrated up to the first tropopause, or the lowest tropopause. The magnitudes of the bias in TCO between NCEP-based estimates and ozonesonde-based estimates was only 1.2 DU, with a standard deviation of 2.3 DU. Thus, we neglected the difference resulting from the tropopause height definition in the climatological analysis of TCO, such as seasonal variation ranging from 20 to 50 DU. Randel et al. (2007) reported that ozone profiles with double tropopauses exhibit systematically less ozone than those with single tropopause in the lower stratosphere. Double tropopauses are associated with strong cyclonic circulation systems, and thus we have to reexamine the tropopause definition carefully when investigating short-term variation as presented in Subsection 3.3.

6. Conclusions

This study focused on tropospheric column ozone (TCO) data observed by satellite instruments over East Asia to investigate the origin of tropospheric ozone. This paper presents the first analysis of long-term variation in the E-TCO and the STJ on daily, monthly, and seasonal timescales using a long-term record of observation: two satellite-based datasets (GOME- and OMI/MLS-derived TCO data) and ozonesonde-derived TCO data.

The two satellite-based datasets showed that the E-TCO belt was observed from 1995 to 2009 with seasonal variation of latitudes; it moved north from winter to summer and south from summer to winter. The E-TCO belt was located close to the STJ throughout the year. According to the CHASER simulation for East Asia, ozone of tropospheric origin and that of stratospheric origin are maximal at similar latitudes. For both, the peak latitudes shift north in summer and south in winter. The simulations indicate that the contribution of ozone of tropospheric origin to the E-TCO belt is, at least, comparable with that of stratospheric origin. However, the peak latitude of TCO is close to the latitude at which the ozone of stratospheric origin peaks. This is because the ozone of stratospheric origin, which is limited to near the STJ throughout the year, has a steeper latitudinal gradient. The enhancement of TCO near the STJ does not necessarily indicate that the ozone of stratospheric origin is dominant. As the simulations indicate, the observed enhancement of TCO over East Asia can be interpreted as the overlapped contributions from the two origins: intrusion from the stratosphere near the STJ and photochemical production in the troposphere.

Moreover, our results suggest that in East Asia, where the source regions of anthropogenic ozone precursors are located at similar latitudes to the STJ, photochemically produced ozone can be masked by ozone from the stratosphere in TCO observations from satellites. In fact, some daily TCO data derived from GOME measurements showed that enhanced ozone over polluted areas (e.g., central China) was separated from the STJ, demonstrating photochemical production of ozone.

Acknowledgements

Programs for determining the ozonesonde-based tropopause height were provided by Dr. Katsuyuki Noguchi. We thank Dr. Makoto Kuji for helpful discussions. This research was supported by the Grant-in-Aid for Scientific Research (C) 21540454 by the Japan Society for the Promotion of Science (JSPS) and the Global Environment Research Fund (S-7) by the Ministry of the Environment (MOE), Japan. The CHASER calculations were performed on the NIES supercomputer system (NEC SX-8R). Research at the SAO was supported by NASA and the Smithsonian Institution.

Appendix

OMI/MLS-derived TCO and the ozonesonde-derived TCO are here denoted as $I_{\mathrm{OMI/MLS}}$ and I_{sonde}, respectively. Biases in $I_{\mathrm{OMI/MLS}}$, denoted as B, were defined at each ozonesonde station during the observation period (2004–2009) as:

$$B = \frac{\sum_{i=1}^{N} \Delta I^{i}_{OMI/MLS}}{N} = \Delta \bar{I}_{OMI/MLS}$$

where $\Delta I^{i}_{OMI/MLS} = I^{i}_{OMI/MLS} - I^{i}_{sonde}$. Standard deviations in $I_{OMI/MLS}$ at each ozonesonde station during the observation period, denoted as σ, were defined as the

standard deviations of $\Delta I_{OMI/MLS}$: i.e.,

$$\sigma = \sqrt{\frac{\sum_{i=1}^{N}\left(\Delta I^{i}_{OMI/MLS} - \Delta \bar{I}_{OMI/MLS}\right)^{2}}{N}}.$$

References

Akiyoshi, H., L. B. Zhou, Y. Yamashita, K. Sakamoto, M. Yoshiki, T. Nagashima, M. Takahashi, J. Kurokawa, M. Takigawa, and T. Imamura, 2009: A CCM simulation of the breakup of the 20 Antarctic polar vortex in the years 1980–2004 under the CCMVal scenarios. *J. Geophys. Res.*, **114**, 3103–3130.

Andreae, M. O., P. Artaxo, H. Fischer, S. R. Freitas, J.-M. Grégoire, A. Hansel, P. Hoor, R. Kormann, R. Krejci, L. Lange, J. Lelieveld, W. Lindinger, K. Longo, W. Peters, M. de Reus, B. Scheeren, M. A. F. Silva Dias, J. Ström, P. F. J. van Velthoven, and J. Williams, 2001: Transport of biomass burning smoke to the upper troposphere by deep convection in the equatorial region. *Geophys. Res. Lett.*, **28**, 951–954.

Chandra, S., J. R. Ziemke, and R. V. Martin, 2003: Tropospheric ozone at tropical and middle latitudes derived from TOMS/MLS residual: Comparison with a global model. *J. Geophys. Res.*, **108**, 4291–4309.

de Laat, A. T. J., I. Aben, and G. J. Roelofs, 2005: A model perspective on total tropospheric O_3 column variability and implications for satellite observations. *J. Geophys. Res.*, **110**, 13303–13322.

European Space Agency, 1995: *The GOME Users Manual*, edited by F. Bednarz, ESA Spec. Publ. SP-1182.

Fishman, J., P. Minnis, and H. G. Reichle, Jr., 1986: Use of satellite data to study tropospheric ozone in the tropics. *J. Geophys. Res.*, **91**, 14451–14465.

Fishman, J., and J. C. Larsen, 1987: Distribution of total ozone and stratospheric ozone in the tropics: Implications for the distribution of tropospheric ozone. *J. Geophys. Res.*, **92**, 6627–6634.

Fishman, J., C. E. Watson, J. C. Larsen, and J. A. Logan, 1990: Distribution of tropospheric ozone determined from satellite data. *J. Geophys. Res.*, **95**, 3599–3617.

Fishman, J., A. E. Wozniak, and J. K. Creilson, 2003: Global distribution of tropospheric ozone from satellite measurements using the empirically corrected tropospheric ozone residual technique: Identification of the regional aspects of air pollution. *Atmos. Chem. Phys.*, **3**, 893–907.

Hayashida, S., N. Urita, K. Noguchi, X. Liu, and K. Chance, 2008: Spatiotemporal variation in tropospheric column ozone over East Asia observed by GOME and ozonesondes. *SOLA*, **4**, 117–120.

Holton, J. R., P. H. Haynes, M. E. Mcintyre, A. R. Douglass, R. B. Rood, and L. Pfister, 1995: Stratosphere-Troposphere Exchange. *Rev. Geophys.*, **33**, 403–439.

Hsu J., M. J. Prather, and O. Wild, 2005: Diagnosing the stratosphere-to-troposphere flux of ozone in a chemistry transport model. *J. Geophys. Res.*, **110**, 19305–19317.

IPCC, 2007: A report of Working Group I of the Intergovernmental Panel on Climate Change.

Krishnamurti, T. N., M. C. Sinha, M. Kanamitsu, D. Oosterhof, H. Fuelberg, R. Chatfield, D. J. Jacob, and J. Logan, 1996: Passive tracer transport relevant to the TRACE A experiment. *J. Geophys. Res.*, **101**, 23889–23908.

Lee, S., Y. Hong, C. Song, M. Lee, S. Ryoo, J. Kim, S. Yong, P. K. Bhartia, R. Park, J. Woo, Y. J. Kim, C. H. Song, J. H. Kim, K. Lee, C. Ho, S. K. Park, Y. Lee, J. Lee, M. Kim, Y. Eom, and J. Hong, 2009: Geostationary Environment Monitoring Spectrometer (GEMS) onboard MP-GEOSAT (Multi Purpose Geostationary Satellite) over Asia-Pacific region. *Eos, Trans. Amer. Geophys. Union*, **90**, Fall Meet. Suppl., Abstract A553A-0251.

Lelieveld, J., and F. J. Dentener, 2000: What controls tropospheric ozone? *J. Geophys. Res.*, **105**, 3531–3551.

Levelt, P. F., G. H. J. van den Oord, M. R. Dobber, A. Malkki, H. Visser, J. de Vries, P. Stammes, J. O. V. Lundell, and H. Saari, 2006: The Ozone Monitoring Instrument. *IEEE Trans. Geosci. Remote Sens.*, **44**, 1093–1101.

Liu, X., K. Chance, C. E. Sioris, R. J. D. Spurr, T. P. Kurosu, R. V. Martin, and M. J. Newchurch, 2005: Ozone profile and tropospheric ozone retrievals from the Global Ozone Monitoring Experiment: Algorithm description and validation. *J. Geophys. Res.*, **110**, 20307–20325.

Liu, X., K. Chance, C. E. Sioris, T. P. Kurosu, R. J. D. Spurr, R. V. Martin, T.-M. Fu, J. A. Logan, D. J. Jacob, P. I. Palmer, M. J. Newchurch, I. A. Megretskaia, and R. B. Chatfield, 2006: First directly retrieved global distribution of tropospheric column ozone from GOME: Comparison with the GEOS-CHEM model. *J. Geophys. Res.*, **111**, 2308–2324.

Logan, J. A., 1999: An analysis of ozonesonde data for the troposphere: Recommendations for testing 3-D models and development of a gridded climatology for tropospheric ozone. *J. Geophys. Res.*, **104**, 16115–16149.

Martin, R. V., D. J. Jacob, J. A. Logan, I. Bey, R. M. Yantosca, A. C. Staudt, Q. Li, A. M. Fiore, B. N. Duncan, and H. Liu, 2002: Interpretation of TOMS observations of tropical tropospheric ozone with a global model and in-situ observations. *J. Geophys. Res.*, **107**, 4351–4383.

McPeters, R. D., J. A. Logan, and G. J. Labow, 2003: Ozone climatological profiles for version 8 TOMS and SBUV retrievals. *Eos, Trans. Amer. Geophys. Union*, **84**, Fall Meet. Suppl., Abstract A21D-0998.

Meyer-Arnek, J., A. Ladstätter-Weißenmayer, A. Richter, F. Wittrock, and J. P. Burrows, 2005: A study of the trace gas columns of O_3, NO_2 and HCHO over Africa in September 1997. *Faraday Discuss.*, **130**, 387–405.

Nagashima, T., T. Ohara, K. Sudo, and H. Akimoto, 2010: The relative importance of various source regions on East Asian surface ozone. *Atmos. Chem. Phys. Discuss.*, **10**, 9077–9120.

Noguchi K., N. Urita, S. Hayashida, X. Liu, and K. Chance, 2007: Validation and comparison of tropospheric column ozone derived from GOME measurements with ozonesondes over Japan. *SOLA*, **3**, 41–44.

Ohara, T., H. Akimoto, J. Kurokawa, N. Horii, K. Yamaji, X. Yan, and T. Hayasaka, 2007: An Asian emission inventory of anthropogenic emission sources for the period 1980–2020. *Atmos. Chem. Phys.*, **7**, 4419–4444.

Pickering, K. E., A. M. Thompson, Y. Wang, W.-K. Tao, D. P. McNamara, V. W. J. H. Kirchhoff, B. G. Heikes, G. W. Sachse, J. D. Bradshaw, G. L. Gregory, and D. R. Blake, 1996: Convective transport of biomass burning emissions over Brazil during TRACE A. *J. Geophys. Res.*, **101**, 23993–24012.

Randel, W. J., D. J. Seidel, and L. L. Pan, 2007: Observational characteristics of double tropopauses. *J. Geophys. Res.*, **112**, D07309, doi:10.1029/2006JD007904.

Sauvage, B., R. V. Martin, A. van Donkelaar, and J. R. Ziemke, 2007: Quantification of the factors controlling tropical tropospheric ozone and the South Atlantic maximum. *J. Geophys. Res.*, **112**, 11309–11322.

Schoeberl, M. R., J. R. Ziemke, B. Bojkov, N. Livesey, B. Duncan, S. Strahan, L. Froidevaux, S. Kulawik, P. K. Bhartia, S. Chandra, P. F. Levelt, J. C. Witte, A. M. Thompson, E. Cuevas, A. Redondas, D. W. Tarasick, J. Davies, G. Bodeker, G. Hansen, B. J. Johnson, S. J. Oltmans, H. Vömel, M. Allaart, H. Kelder, M. Newchurch, S. Godin-Beekmann, G. Ancellet, H. Claude, S. B. Andersen, E. Kyrö, M. Parrondos, M. Yela, G. Zablocki, D. Moore, H. Dier, P. von der Gathen, P. Viatte, R. Stübi, B. Calpini, P. Skrivankova, V. Dorokhov, H. de Backer, F. J. Schmidlin, G. Coetzee, M. Fujiwara, V. Thouret, F. Posny, G. Morris, J. Merrill, C. P. Leong, G. Koenig-Langlo, and E. Joseph, 2007: A trajectory-based estimate of the tropospheric ozone column using the residual method. *J. Geophys. Res.*, **112**, D24S49, doi:10.1029/2007JD008773.

Stajner, I., K. Wargan, S. Pawson, H. Hayashi, L. Chang, R. C. Hudman, L. Froidevaux, N. Livesey, P. F. Levelt, A. M. Thompson, D. W. Tarasick, R. Stübi, S. B. Andersen, M. Yela, G. K.-Langlo, F. J. Schmidlin, and J. C. Witte, 2008: Assimilated ozone from EOS-Aura: Evaluation of the tropopause region and tropospheric columns. *J. Geophys. Res.*, **113**, D16S32, doi:10.1029/2007JD008863.

Stevenson, D. S., F. J. Dentener, M. G. Schultz, K. Ellingsen, T. P. C. van Noije, O. Wild, G. Zeng, M. Amann, C. S. Atherton, N. Bell, D. J. Bergmann, I. Bey, T. Butler, J. Cofala, W. J. Collins, R. G. Derwent, R. M. Doherty, J. Drevet, H. J. Eskes, A. M. Fiore, M. Gauss, D. A. Hauglustaine, L. W. Horowitz, I. S. A. Isaksen, M. C. Krol, J.-F. Lamarque, M. G. Lawrence, V. Montanaro, J.-F. Müller, G. Pitari, M. J. Prather, J. A. Pyle, S. Rast, J. M. Rodriguez, M. G. Sanderson, N. H. Savage, D. T. Shindell, S. E. Strahan, K. Sudo, and S. Szopa, 2006: Multimodel ensemble simulations of present-day and near-future tropospheric ozone. *J. Geophys. Res.*, **111**, D08301, doi:10.1029/2005JD006338

Streets, D. G., T. C. Bond, G. R. Carmichael, S. D. Fernandes, Q. Fu, D. He, Z. Klimont, S. M. Nelson, N. Y. Tsai, M. Q. Wang, J.-H. Woo, and K. F. Yarber, 2003: An inventory of gaseous and primary aerosol emissions in Asia in the year 2000. *J. Geophys. Res.*, **108**, 8809, doi:10.1029/2002JD003093.

Sudo, K., and H. Akimoto, 2007: Global source attribution of tropospheric ozone: Long-range transport from various source regions. *J. Geophys. Res.*, **112**, 12302–12322.

Sudo, K., M. Takahashi, J. Kurokawa, and H. Akimoto, 2002: CHASER: A global chemical model of the troposphere: 1. Model description. *J. Geophys. Res.*, **107**, 4339–4358.

Takigawa, M., M. Takahashi, and H. Akiyoshi, 1999: Simulation of ozone and other chemical species using a Center for Climate System Research/National Institute for Environmental Studies atmospheric GCM with coupled stratospheric chemistry. *J. Geophys. Res.*, **104**, 14003–14018.

Thompson, A. M., and Hudson, R. D., 1999: Tropical tropospheric ozone (TTO) maps from Nimbus 7 and Earth Probe TOMS by the modified-residual method: Evaluation with sondes, ENSO signals, and trends from Atlantic regional time series. *J. Geophys. Res.*, **104**, 26961–26975.

Wang, Y., D. J. Jacob, and J. A. Logan, 1998: Global simulation of tropospheric O_3-NO_x-hydrocarbon chemistry: 1. Model formulation. *J. Geophys. Res.*, **103**, 10713–1072.

Waters, J. W., L. Froidevaux, R. S. Harwood, R. F. Jarnot, H. M. Pickett, W. G. Read, P. H. Siegel, R. E. Cofield, M. J. Filipiak, D. A. Flower, J. R. Holden, G. K. Lau, N. J. Livesey, G. L. Manney, H. C. Pumphrey, M. L. Santee, D. L. Wu, D. T. Cuddy, R. R. Lay, M. S. Loo, V. S. Perun, M. J. Schwartz, P. C. Stek, R. P. Thurstans, M. A. Boyles, S. Chandra, M. C. Chavez, G.-S. Chen, B. V. Chudasama, R. Dodge, R. A. Fuller, M. A. Girard, J. H. Jiang, Y. Jiang, B. W. Knosp, R. C. LaBelle, J. C. Lam, K. A. Lee, D. Miller, J. E. Oswald, N. C. Patel, D. M. Pukala, O. Quintero, D. M. Scaff, W. V. Snyder, M. C. Tope, P. A. Wagner, and M. J. Walch, 2006: The Earth Observing System Microwave Limb Sounder (EOS MLS) on the Aura satellite. *IEEE Trans. Geosci. Remote Sens.*, **44**, no. 5.

Worden, H. M., J. A. Logan, J. R. Worden, R. Beer, K. Bowman, S. A. Clough, A. Eldering, B. M. Fisher, M. R. Gunson, R. L. Herman, S. S. Kulawik, M. C. Lampel, M. Luo, I. A. Megretskaia, G. B. Osterman, and M. W. Shephard, 2007: Comparisons of Tropospheric Emission Spectrometer (TES) ozone profiles to ozonesondes: Methods and initial results. *J. Geophys. Res.*, **112**, D03309, doi:10.1029/2006JD007258.

Yang, Q., D. M. Cunnold, H.-J. Wang, L. Froidevaux, H. Claude, J. Merrill, M. Newchurch, and S. J. Oltmans, 2007: Midlatitude tropospheric ozone columns derived

from the Aura Ozone Monitoring Instrument and Microwave Limb Sounder measurements. *J. Geophys. Res.*, **112**, D20305, doi:10.1029/2007JD008528.

Ziemke, J. R., S. Chandra, B. N. Duncan, L. Froidevaux, P. K. Bhartia, P. F. Levelt, and J. W. Waters, 2006: Tropospheric ozone determined from Aura OMI and MLS: Evaluation of measurements and comparison with the Global Modeling Initiative's Chemical Transport Model. *J. Geophys. Res.*, **111**, 19303–19320.

Zhang, Q., D. G. Streets, G. R. Carmichael, K. B. He, H. Huo, A. Kannari, Z. Klimont, I. S. Park, S. Reddy, J. S. Fu, D. Chen, L. Duan, Y. Lei, L. T. Wang, and Z. L. Yao, 2009: Asian emissions in 2006 for the NASA INTEX-B mission. *Atmos. Chem. Phys.*, **9**, 5131–5153.